

Supporting Information

Colloidal Assembly and 3D Shaping by Dielectrophoretic Confinement

Ahmet F. Demirörs*^[a] Jérôme J. Crassous*^[b]

^[a] Complex Materials, Department of Materials, ETH Zurich, 8093 Zurich, Switzerland

E-mail: ahmet.demiroers@mat.ethz.ch

^[b] Physical Chemistry, Chemical Center, Lund University, PO BOX 124, SE-22210 Lund, Sweden

E-mail: jerome.crassous@fkem1.lu.se

Here, we provide extra information first of all for the **DEP pool** configuration, where we have one micro-fabricated electrode with a plane counter electrode. We start by finite element calculations of the electric field and electric field gradient for a micro-fabricated electrode with a square geometry and also demonstrate evaluation of field and field gradient over space (S1). We then show the random hexagonal close packed (*rhcp*) phase formation for colloids at **DEP pool** configuration at moderate field strengths (S2). At S3 we further address how well the simulations and the experiments correlate, by demonstrating the field and the corresponding assembly in different planes of the assembly. We extend the simulations of the field to electrodes that possess various-shaped-voids in S4. Starting from S5 we divert our focus on **DEP hourglass** configurations and at S5 we provide finite element calculations for the **DEP hourglass** configuration obtained by using square-voided electrodes (S5-1). In addition, here, we address the influence of distance between the electrodes (S5-2) and the influence of void size (S5-3) to the field gradient formed in **DEP hourglass** systems. At S6 we provide 3D microscopy image reconstructions to demonstrate the influence of particle volume fraction and field strength on the shape of the 3D assembly. At S7 we demonstrate the influence of field strength and volume fraction to the shape of the assembly by fixing the assembly and imaging either by confocal microscopy or SEM. At S8 finite element calculations of the electric field is given for **DEP hourglass** configuration of distinct electrodes on the two sides.

S1. Finite element calculations of the electric field in the *DEP pool* configuration used in Figure 2a-c.

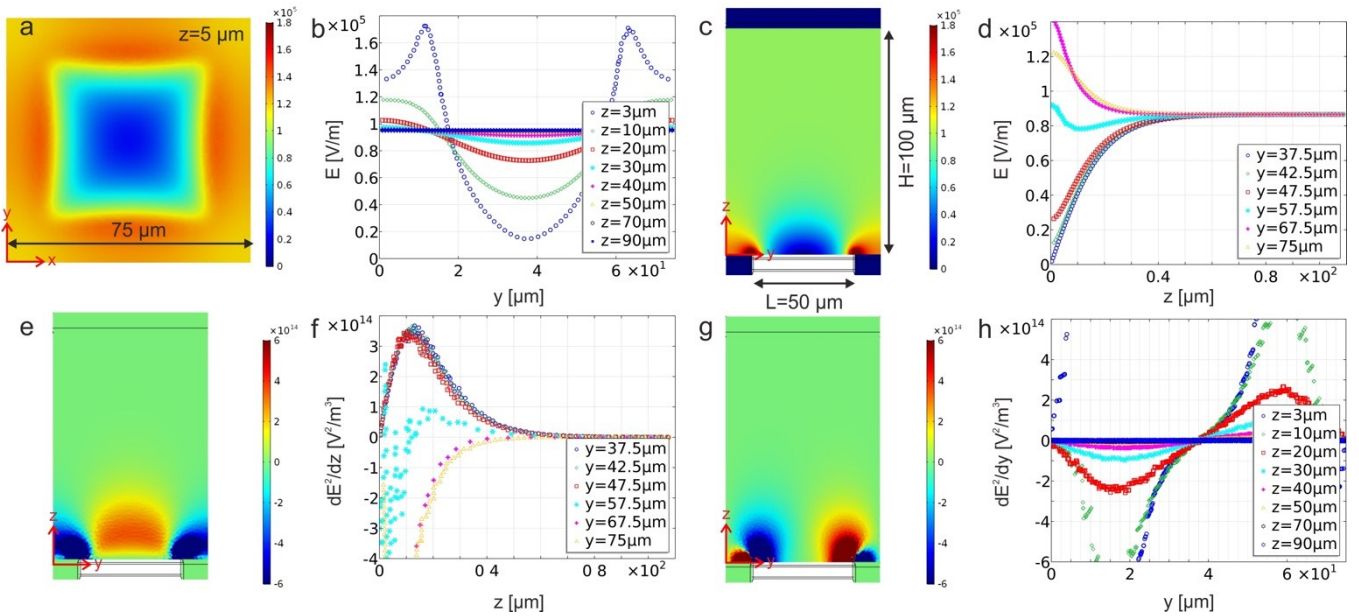


Figure S1. Field calculation in a *DEP pool* configuration. Finite element calculations of the electric field created by a patterned electrode with $50 \mu\text{m}$ square voids and a $75 \mu\text{m}$ pitch facing a plain electrode separated by $110 \mu\text{m}$ under an applied field of $0.1 \text{ V}\mu\text{m}^{-1}$. (a) Top view of the electric field at $z = 5 \mu\text{m}$. (b) Evolution of the field E [V m^{-1}] across the voids evaluated at different heights. (c) Side view of the corresponding electric field and (d) evaluation of the field across the gap from the center of the void ($y = 37.5 \mu\text{m}$) to the periphery where the two gold surfaces face each other ($y = 75 \mu\text{m}$). (e) Side view of the field gradient dE^2/dz [V²/m³] and (f) its evaluation across the gap. (g) Same calculation for dE^2/dy and (h) its evaluation at different z -values shown in (b).

S2. Assemblies in *rhcp* lattices observed with star- and cross- micropatterned electrodes at intermediate field strengths.

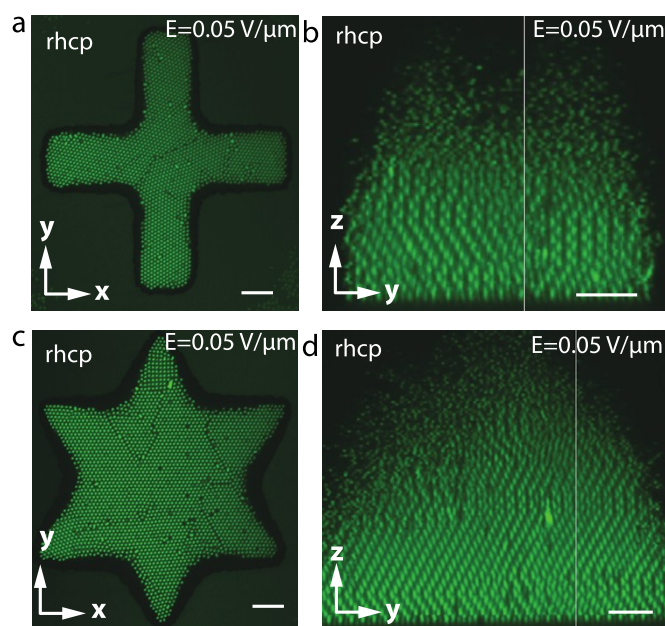


Figure S2. (a,b) Top and side views of the *rhcp* assembly observed with a cross-patterned electrode using a 3 vol% dispersion (radius of the particle $R=0.55 \mu\text{m}$) at a field strength of $0.05 \text{ V}/\mu\text{m}^{-1}$. (c,d) Top and side views of the *rhcp* assembly observed for a star-patterned electrode under similar condition. Scale bars are $5 \mu\text{m}$.

S3. Global view of the assemblies observed using micropatterned electrodes with different feature geometries.

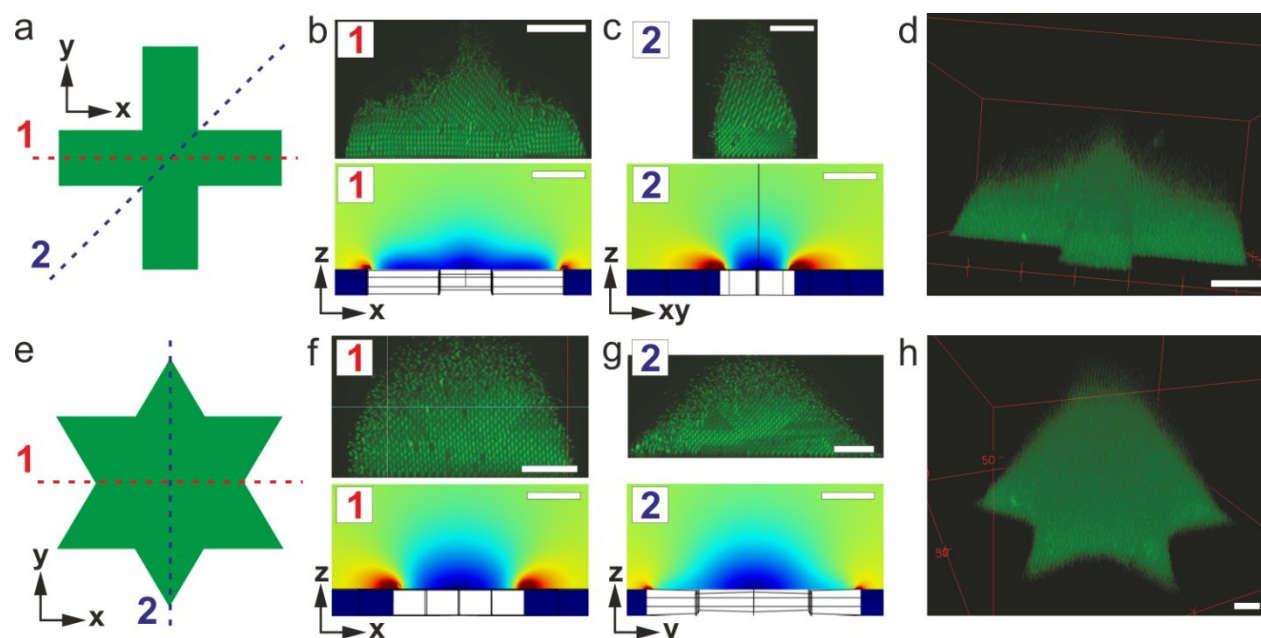


Figure S3. (a) Cross-pattern together with two characteristic cross-sections drawn as dashed lines. (b,c) Micrographs of the assembly performed on a 3 vol% dispersion at $0.07 \text{ V}/\mu\text{m}^{-1}$ following the two cross-sections compared to finite element calculations of the local electric field. (d) 3D CLSM reconstruction of the assembly. (e) Star-pattern together with two characteristic cross-sections drawn as dashed lines. (f,g) Micrographs of the assembly performed on a 3 vol% dispersion at $0.07 \text{ V}/\mu\text{m}^{-1}$ following the two cross-sections compared to finite element calculations of the local electric field. (h) 3D CLSM reconstruction of the assembly. Scale bars are $20 \mu\text{m}$ in simulation graphs and $10 \mu\text{m}$ in experimental graphs.

S4. Finite element calculations of the electric field generated by electrodes with different feature geometries.

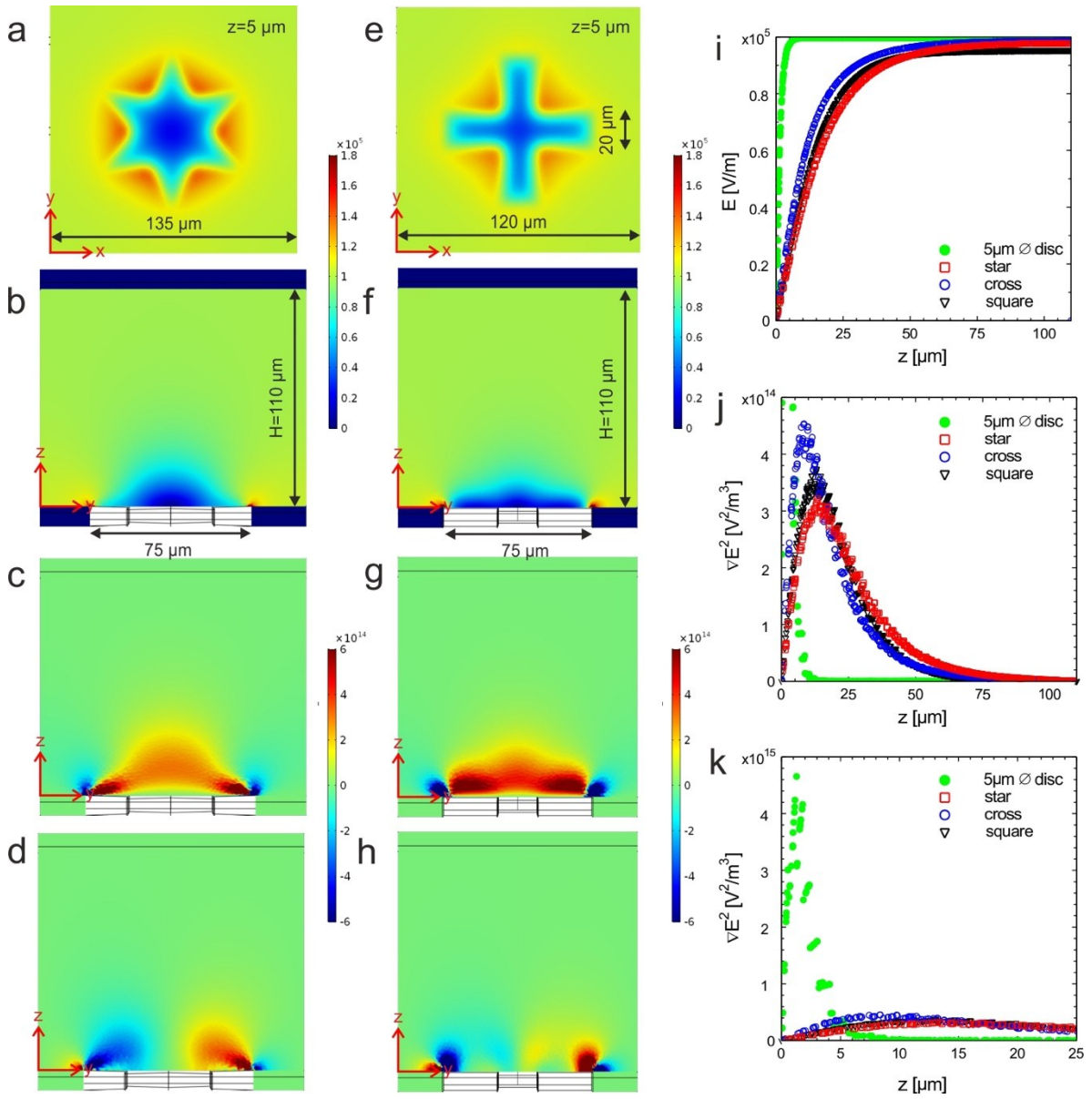


Figure S4. (a-d) Finite element calculation of the field and field gradient generated by a star patterned electrode used in **Figure 2** with a pitch of 135 μm facing a plain electrode separated by a distance $H=110$ μm ((a,b) E [V/m] top and side view, (c) dE^2/dz [V^2/m^3], (d) dE^2/dy [V^2/m^3]). (e-h) Same calculations for the experiment on the cross patterned electrode presented in **Figure 2**. (i) Evaluation of the electric field at the center of the void for the different patterns used in the experiments in **Figure 1** and **Figure 2**. (j,k) Evaluation of dE^2/dz for the different geometries with different scales.

S5. Finite element calculations of the electric field in the *DEP hourglass* configuration.

S5-1. Finite element field calculation corresponding to the configuration used in Figure 3 a-n.

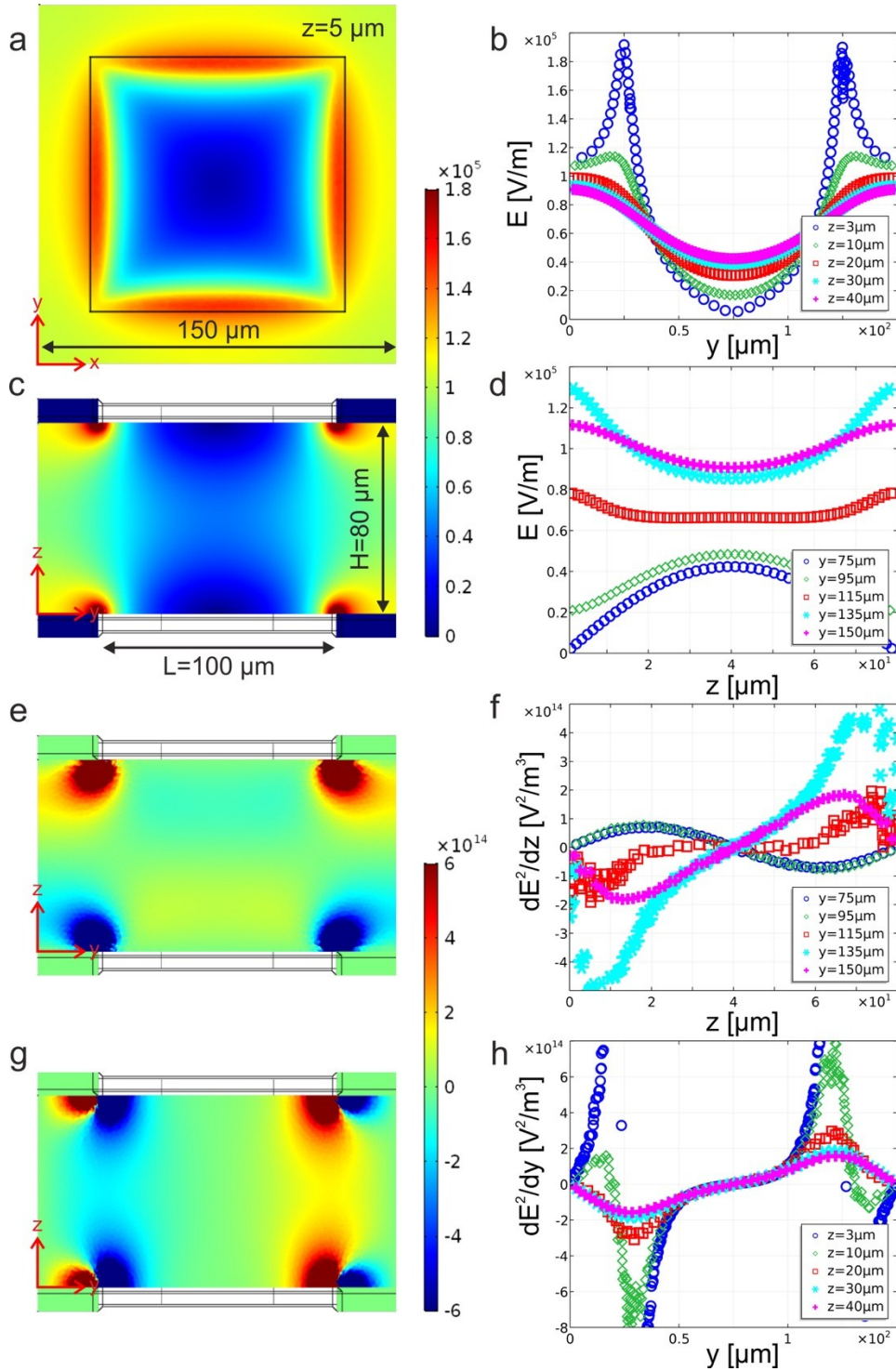


Figure S5. Finite element calculations of the electric field created by two facing patterned electrodes with $100 \mu\text{m}$ square voids and a $200 \mu\text{m}$ pitch separated by $100 \mu\text{m}$ after applying an electric potential of 10 V to the upper electrode ($E_{\text{app}} = 0.1 \text{ V}\mu\text{m}^{-1}$). **(a)** Top view of the electric field at $z = 5 \mu\text{m}$. **(b)** Evolution of the field $E \text{ [V/m]}$ across the voids evaluated at different heights. **(c)** Side view of the corresponding electric field and **(d)** evaluation of the field across the gap from the center of the void ($y = 75 \mu\text{m}$) to the periphery where the two gold surfaces face each other ($y = 150 \mu\text{m}$). **(e)** Side view of the field gradient $dE^2/dz \text{ [V}^2/\text{m}^3]$ and **(f)** its evaluation across the gap. **(g)** Same calculation for dE^2/dy and **(h)** its evaluation at different z -values.

S5-2. Influence of the distance between the electrodes.

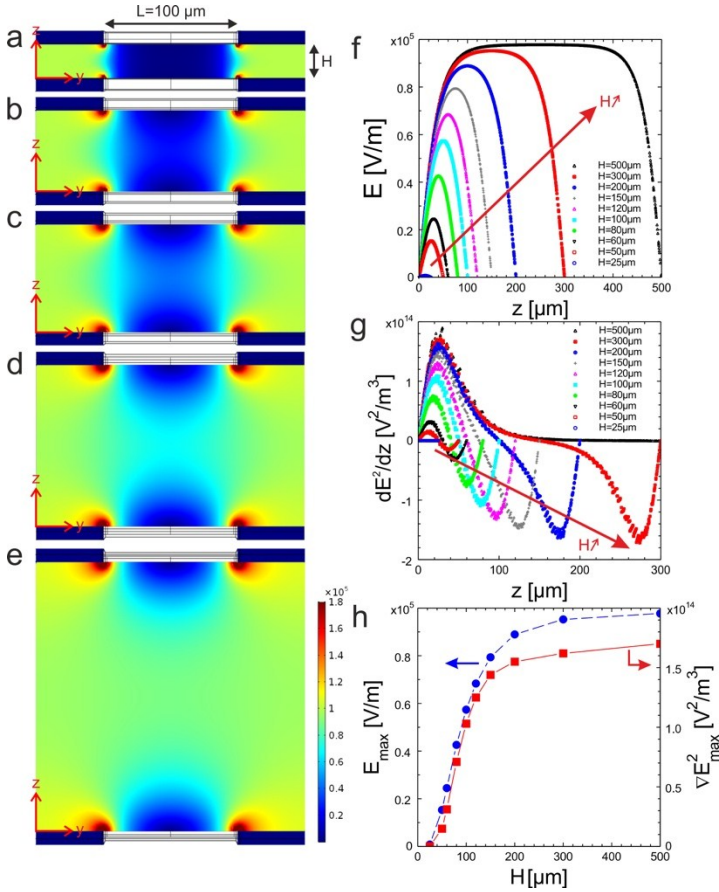


Figure S6. (a-e) Finite element calculations of the field E [Vm^{-1}] generated by two facing square patterned electrodes ($L = 100 \mu\text{m}$, $200 \mu\text{m}$ pitch) as function of their separation distance H at constant applied field ($E_{\text{app}} = 0.1 \text{V}\mu\text{m}^{-1}$) ((a) $25 \mu\text{m}$, (b) $60 \mu\text{m}$, (c) $80 \mu\text{m}$, (d) $120 \mu\text{m}$ and (e) $200 \mu\text{m}$). (f,g) Evaluations of E [Vm^{-1}] and ∇E^2 [V^2m^{-3}] in the center of the void along z -axis. (h) Determination of the maximum field strength E_{max} and squared field gradient ∇E^2_{max} in the center of the geometry as function of the distance between the facing electrodes.

S5-3. Influence of the size of the voids.

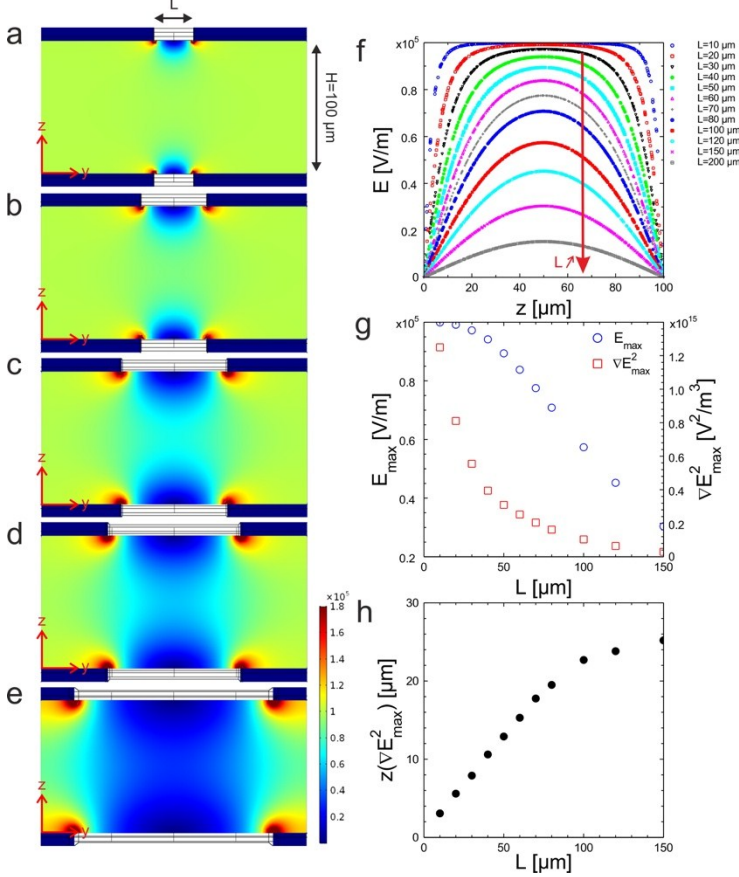


Figure S7. (a-e) Finite element calculations of the field E [Vm^{-1}] generated by two facing square patterned electrodes ($H = 100 \mu\text{m}$, $200 \mu\text{m}$ pitch) as function of the square void size defined by L at constant applied field ($E_{\text{app}} = 0.1 \text{V}\mu\text{m}^{-1}$) ((a) $20 \mu\text{m}$, (b) $50 \mu\text{m}$, (c) $80 \mu\text{m}$, (d) $100 \mu\text{m}$ and (e) $150 \mu\text{m}$). (f) Evaluation of E [Vm^{-1}] in the center of the void for different values of L . (g) Determination of the maximum field strength E_{max} and squared field gradient ∇E^2_{max} in the center of the geometry as function of square size, L . (h) Influence of L to the position where the maximum field gradient is observed (along z -axis in the

S6. Three dimensional reproduction of colloid assembly in the *DEP hourglass* configuration at various electric fields and particle volume fractions.

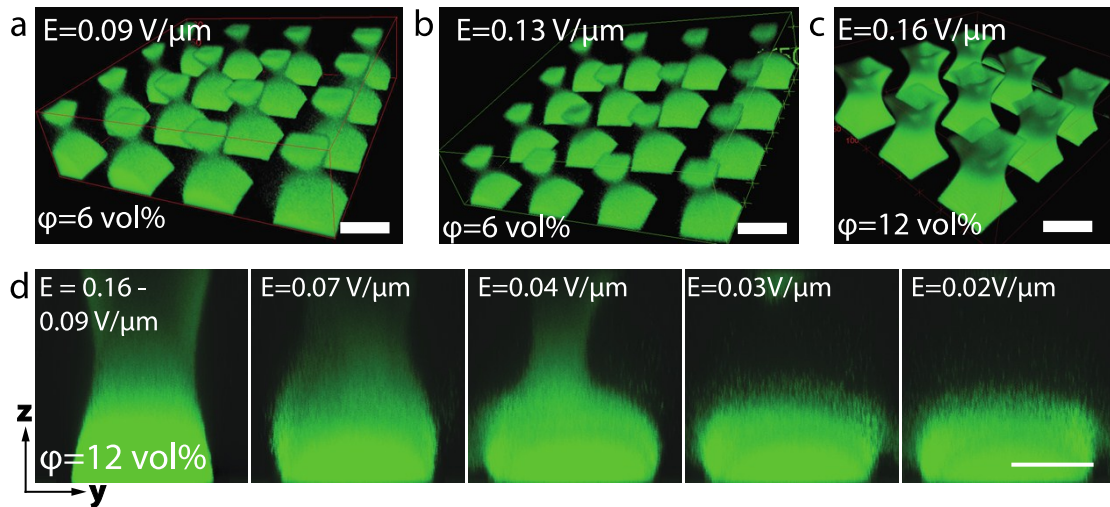


Figure S8. Directed self-assembly in a DEP hourglass configuration using square patterned electrodes ($100 \times 100 \mu\text{m}^2$ square voids with a pitch of $150 \mu\text{m}$, $H = 80 \mu\text{m}$). (a,b) 3D CLSM reconstructions obtained for a 6 vol% dispersion at field strengths of 0.09 and $0.13 \text{ V}\mu\text{m}^{-1}$, respectively. (c) 3D reconstruction of a 12 vol% dispersion at $0.16 \text{ V}\mu\text{m}^{-1}$. The 3D shape results due to the balance between forces generated by the local electric field and gravitational forces. The 3D shape of the assembly is dependent on the particle concentration and the applied field strength. With sufficient particles and field strength, a column-like assembly is observed (c). However, for low concentrations and at high field strengths the neck was detached and two separate assemblies formed on both electrode sides as shown in (b). (d) The influence of field strength on the shape of the assembly is illustrated by the side view (cross-section) of the assembly while gradually decreasing the field strength.

S7. Influence of particle volume fraction on the shape of the assembly in the *DEP hourglass* configuration with identical electrodes.

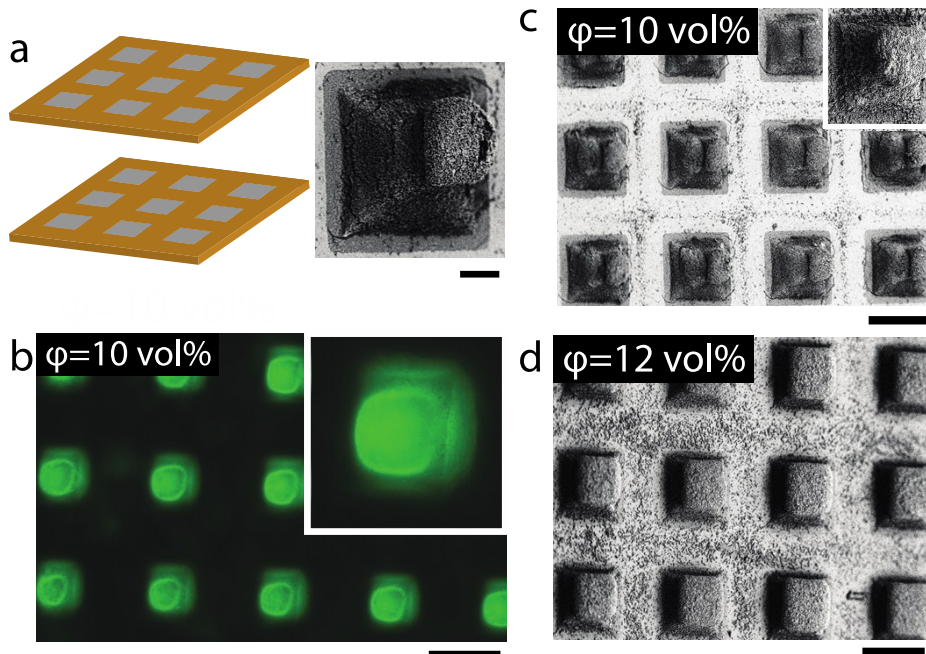


Figure S9. (a) Sample cell design with top- and bottom-electrodes with square-voids ($100 \times 100 \mu\text{m}^2$ square voids with a pitch of $150 \mu\text{m}$, $H = 80 \mu\text{m}$). (b) Confocal microscopy 3D reconstruction of the assembly observed on a 10 vol% dispersion at $0.16 \text{ V}\mu\text{m}^{-1}$. (c) Corresponding SEM micrographs of the truncated-square-pyramidal assembly obtained after polymerization and calcination of the structure. (d) When the particle concentration is increased to $\phi = 12 \text{ vol}\%$ under similar field strength, the shape of the assembly within the voids turns to a rectangular prism as shown by SEM micrographs. Scale bars are $100 \mu\text{m}$ in b, c, d and $10 \mu\text{m}$ in a.

S8. Finite element calculations of the electric field in the *DEP hourglass* configuration with distinct electrodes.

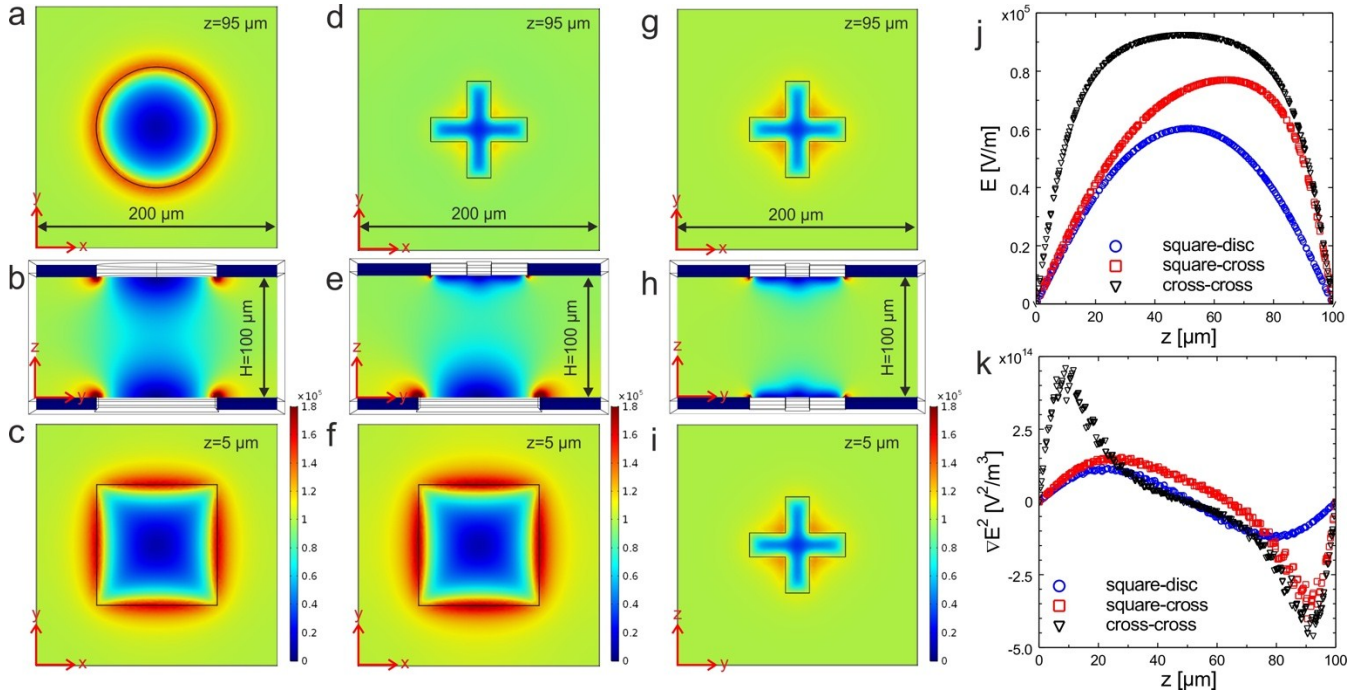


Figure S10. (a-c) Calculations of the field generated by a patterned square electrode ($L = 100 \mu\text{m}$, $200 \mu\text{m}$ pitch) aligned to a disc patterned electrode ($100 \mu\text{m}$ diameter) separated by $H = 100 \mu\text{m}$ ((a) top view: field at $z = 95 \mu\text{m}$, (b) side view in the middle of the geometry, (c) bottom view at $z = 5 \mu\text{m}$). (d-f) Similar calculations for a square-cross configuration. (g-i) Similar calculations for a cross-cross configuration. (f,g) Evaluations of E [Vm^{-1}] and ∇E^2 [V^2m^{-3}] in the center of the geometry for the three configurations.

Supplementary Videos:

Supplementary Video 1:

Assembly of colloids in small round voids of $5 \mu\text{m}$ size at an electric field strength of $0.2\text{V}/\mu\text{m}$ is shown by scanning through the focal plane of imaging starting from the microfabricated electrode surface towards the other plane electrode.

Supplementary Video 2:

Assembly in a *DEP hourglass* configuration with a square-voided electrode on one side and cross-voided electrode, shown also in **Figure 4f** in main text. Here, a 360° rotation of the 3D reconstruction of the assembly is given.